







μ SR measurements on Sr_2RuO_4 under $\langle 110 \rangle$ uniaxial stress

Vadim Grinenko ^{1,2,*}, Rajib Sarkar,¹ Shreenanda Ghosh,^{1,3} Debarchan Das ⁴, Zurab Guguchia,⁴ Hubertus Luetkens,⁴ Ilya Shipulin ⁵, Aline Ramires ⁶, Naoki Kikugawa,⁷ Yoshiteru Maeno,^{8,9} Kousuke Ishida ¹⁰, Clifford W. Hicks ^{10,11} and Hans-Henning Klaus¹

¹*Institute for Solid State and Materials Physics, Technische Universität Dresden, D-01069 Dresden, Germany*

²*Tsung-Dao Lee Institute, Shanghai Jiao Tong University, Pudong, 201210 Shanghai, China*

³*Institute for Quantum Matter, William H. Miller III Department of Physics and Astronomy, The Johns Hopkins University, Baltimore, Maryland 21218, USA*

⁴*Laboratory for Muon Spin Spectroscopy, Paul Scherrer Institut, CH-5232 Villigen PSI, Switzerland*

⁵*Leibniz Institute for Solid State and Materials Research, D-01069 Dresden, Germany*

⁶*Paul Scherrer Institut, CH-5232 Villigen PSI, Switzerland*

⁷*National Institute for Materials Science, Tsukuba 305-0003, Japan*

⁸*Department of Physics, Kyoto University, Kyoto 606-8502, Japan*

⁹*Toyota Riken – Kyoto-University Research Center (TRiKUC), Kyoto University, Kyoto 606-8501, Japan*

¹⁰*Max Planck Institute for Chemical Physics of Solids, D-01187 Dresden, Germany*

¹¹*School of Physics and Astronomy, University of Birmingham, Birmingham B15 2TT, United Kingdom*



(Received 13 September 2022; revised 6 January 2023; accepted 13 January 2023; published 24 January 2023)

Muon spin rotation/relaxation (μ SR) and polar Kerr effect measurements provide evidence for a time-reversal symmetry breaking (TRSB) superconducting state in Sr_2RuO_4 . However, the absence of a cusp in the superconducting transition temperature (T_c) vs stress and the absence of a resolvable specific heat anomaly at TRSB transition temperature (T_{TRSB}) under uniaxial stress challenge a hypothesis of TRSB superconductivity. Recent μ SR studies under pressure and with disorder indicate that the splitting between T_c and T_{TRSB} occurs only when the structural tetragonal symmetry is broken. To further test such behavior, we measured T_c through susceptibility measurements and T_{TRSB} through μ SR, under uniaxial stress applied along a $\langle 110 \rangle$ lattice direction. We have obtained preliminary evidence for suppression of T_{TRSB} below T_c , at a rate much higher than the suppression rate of T_c .

DOI: [10.1103/PhysRevB.107.024508](https://doi.org/10.1103/PhysRevB.107.024508)

I. INTRODUCTION

Even after nearly 30 years of research, the superconductivity of Sr_2RuO_4 is a mystery [1]. The greatest conundrum is the evidence that the order parameter combines even parity with time-reversal symmetry breaking. The evidence for even parity comes especially from recent NMR measurements [2–4], showing a spin-singlet-like susceptibility drop below T_c . Evidence for time-reversal symmetry breaking (TRSB) comes from anomalous switching noise in junctions [5,6], Kerr rotation [7], and enhanced muon spin relaxation in the superconducting state [8–14].

In previous muon spin rotation/relaxation (μ SR) studies of Sr_2RuO_4 , some of the present authors observed that T_{TRSB} and T_c split under uniaxial stresses applied along a $\langle 100 \rangle$ crystallographic direction, thereby supporting a scenario of TRSB superconductivity [13]. Together with the observation that T_{TRSB} and T_c track each other under hydrostatic stress and also under an introduction of disorder [12], this observation suggests a symmetry-protected even-parity chiral superconducting state, $d_{xz} \pm id_{yz}$. This order parameter would be surprising because the line node at $k_z = 0$ im-

plies, conventionally, interlayer pairing, while the interlayer interactions in Sr_2RuO_4 are expected to be weak given the apparent strong two dimensionality of its electronic structure [15]. Recently, it has been proposed that the superconductivity of Sr_2RuO_4 could emerge through interorbital interactions [16–21]. Pairing in these proposals is primarily driven by local interactions (such as Hund’s coupling), evading the need for strong interlayer coupling and suggesting that chiral d -wave superconductivity could be a rather natural order parameter for Sr_2RuO_4 .

So far, the splitting of the transitions under uniaxial $\langle 100 \rangle$ stress has been seen only in μ SR measurements. In contrast with expectations for a chiral state, a second anomaly was not resolved either in heat capacity [22] nor in elastocaloric effect [23] measurements in which uniaxial stress was applied to split T_c and T_{TRSB} . In addition, the expected cusp in the dependence of T_c on uniaxial stress has not been resolved for either $\langle 100 \rangle$ or $\langle 110 \rangle$ directions. These contradictory results have led to proposals that TRSB in Sr_2RuO_4 is finely tuned with order parameters of the form $s \pm id$, $s \pm ip$ [24,25], or $d \pm ig$ [26,27], or even might occur only in the vicinity of extended defects [28].

For $\langle 100 \rangle$ stress, T_c strongly increases on approach to a van Hove singularity [29], while T_{TRSB} barely changes [13]. The high sensitivity of the electronic structure to $\langle 100 \rangle$ stress

*vadim.a.grinenko@gmail.com

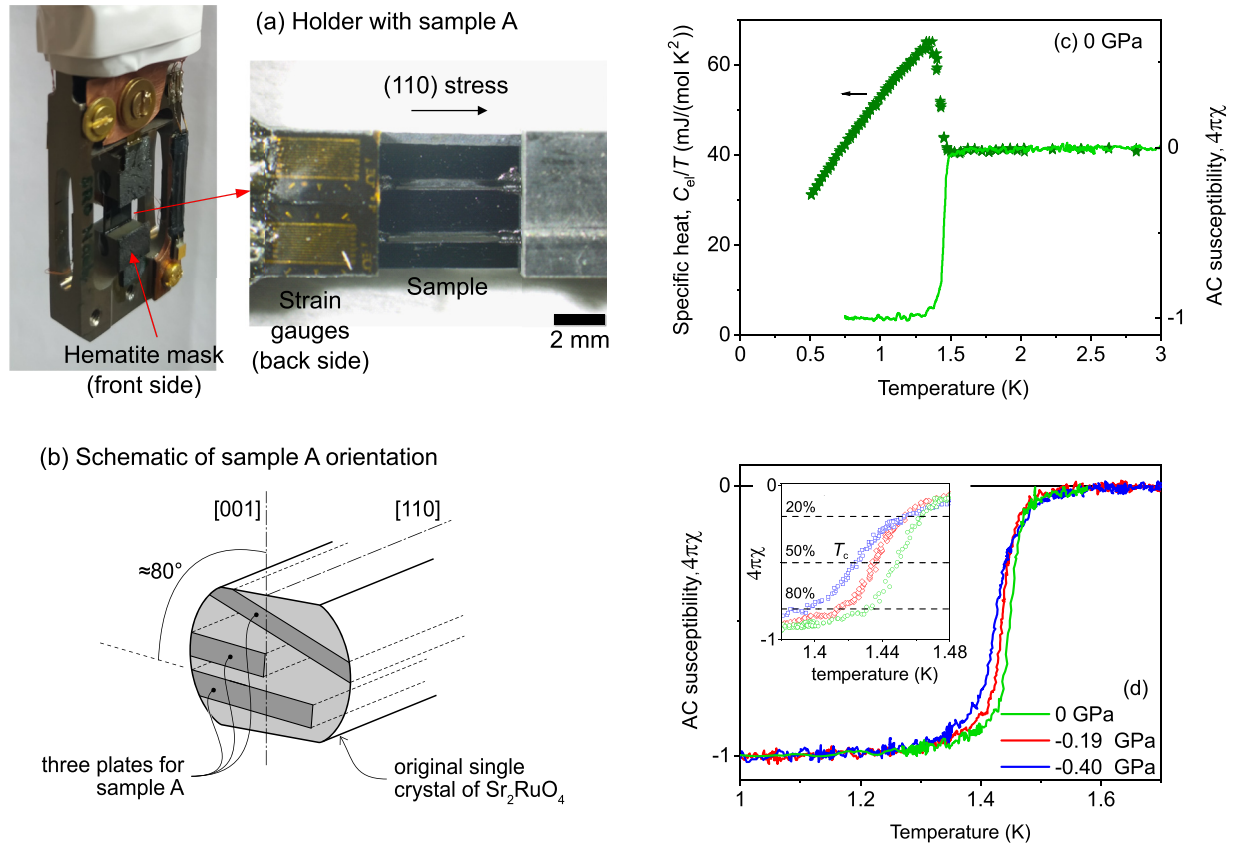


FIG. 1. (a) Photographs of the holder with a mounted sample A consisting of three rectangular-shaped pieces glued into the holder side by side. (Left) The front view of the mounted sample with hematite masks used to screen the portions of the holder in the muon beam. Concentric coils behind the sample (not seen) are used for *in situ* measurements of T_c . (Right) The photograph of the sample from the back side with two glued strain gauges. (b) Schematics of the Sr_2RuO_4 rod cross section illustrating the orientation of the individual pieces, determined by x-ray Laue photos. The misalignment of the pieces regarding the crystallographic c axis is intended to reduce the probability of a cleavage under stress. (c) Comparison of the temperature dependence of the specific heat and *in situ* ac susceptibility measured at zero stress. (d) The temperature dependencies of the *in situ* ac susceptibilities at different applied uniaxial stress. Inset shows zoom of a region close to $T_c = 1.448 \pm 0.015$ K, which we take as the transition midpoint. Heat capacity and transverse-field μSR data show that the samples are fully superconducting, so we identify the extrema of the susceptibility signal as $4\pi\chi = 0$ and -1 .

complicates the interpretation of the observed splitting of the transitions. In contrast, the electronic band structure is less sensitive to stress applied along $\langle 110 \rangle$ axes. Although a weaker dependence on stress is expected, it may be easier to interpret observed effects.

Under the tetragonal lattice symmetry of Sr_2RuO_4 , T_c and T_{TRSB} are expected to split under shear strain ε_6 , which has $\langle 110 \rangle$ principal axes, for a $d_{xz} \pm id_{yz}$ order parameter. In the limit of small strain, the rates of change $|dT_c/d\varepsilon_6|$ and $|dT_{\text{TRSB}}/d\varepsilon_6|$ are inversely proportional to the condensation energies associated with each phase transition [13]. Here, we report measurements of both T_c and T_{TRSB} under uniaxial stress applied along $\langle 110 \rangle$ lattice direction. T_c was measured through magnetic susceptibility and T_{TRSB} through μSR . $\langle 110 \rangle$ stress, in addition applying shear strain, also affects the unit cell volume and lattice constant ratio c/a . The effect of these strain components on T_c and T_{TRSB} was estimated using the elasticity stiffness matrix known from the ultrasound experiments [30] and experimental dependencies of T_c on hydrostatic pressure and uniaxial c -axis strain. We obtained preliminary evidence that T_{TRSB} and T_c split under the $\langle 110 \rangle$ uniaxial stress, with the condensation energy asso-

ciated with the time-reversal symmetry breaking being very small compared to that associated with the superconductivity overall. These are very challenging measurements due to the small size of the signal. We publish a preliminary data set now, because a more authoritative data set might not be possible for some time, mainly due to limited beam time.

II. EXPERIMENTAL DESIGN AND RESULTS

Single crystals of Sr_2RuO_4 were grown by a floating zone method [31]. Data from two samples, labeled A and B, are reported. In order to obtain samples of sufficient length for the uniaxial stress apparatus, samples were cut from a rod that grew nearly along a $\langle 110 \rangle$ lattice direction. The samples studied here were either cleaved or ground into plates, exposing the interior of the as-grown rod to the muon beam.

Samples were mounted into holders using Stycast 2850 epoxy as shown in Ref. [13]. The epoxy layers were generally 50–100 μm thick. Additional steps were taken to improve the chances of reaching high stresses without fracturing the sample. (1) They were cut at a 10° angle with respect to the ab plane, so that shear stresses in the sample

do not align with cleave planes. (2) 10- μm -thick titanium foils were affixed to their surfaces with Stycast 1266 for sample B for mechanical reinforcement. (3) The slots in the holder were chamfered, as shown in Fig. 1(b) of Ref. [13], to smooth the interface between the free and clamped portions of the sample. For further details see Refs. [13,32,33].

The specific heat of a small piece of the crystal remaining after the cutting of the plates for μ SR sample A was measured using the thermal relaxation method in a physical property measurement system (PPMS, Quantum Design). The ac susceptibility of the samples prepared for the μ SR experiments was measured *in situ* using pairs of concentric coils located behind the samples. The coils were wound on each other, one of which was used as excitation and the other as a pickup coil. The applied field for the susceptibility measurements was $\sim 10 \mu\text{T}$. For further details, see Refs. [13,33].

The essential experimental setup was the same as those described in Refs. [13,32,33]. The samples are plates thick enough to stop the muon beam, mounted in a holder that facilitates application of force. A photograph of sample A, mounted in the holder, is shown in Fig. 1(a). Sample A consists of three plates cut from one single crystal, as shown in panel (b). In panel (c) the temperature dependence of the specific heat measured on a small cutoff is compared with the *in situ* susceptibility measurements. There is a good agreement between both sets of measurements with the zero stress $T_c = 1.448 \pm 0.015 \text{ K}$ of sample A, defined as shown in panel (d). We also performed μ SR measurements on sample B, which had similar $T_c = 1.46 \pm 0.09 \text{ K}$, with a slightly broader transition width [Fig. 3(a)]. The high T_c , comparable to that of clean-limit Sr_2RuO_4 [34], and the sharp superconducting transition indicate a high sample quality. The stress values were measured by a set of strain gauges mounted on the uniaxial pressure cell as described in Refs. [13,32,33].

In the μ SR method, spin-polarized muons are implanted into the sample, where each then precesses in its local field. The measured quantity is the decay positron emission asymmetry $A(t)$, which is proportional to the muon spin polarization at time t . In this work, we performed experiments in zero external magnetic field, which was dynamically compensated to fields smaller than $1 \mu\text{T}$. Asymmetry curves $A(t)$ at two temperatures, one above and one well below T_c , are shown in Fig. 2, panels (a)–(c) for zero force and two applied pressures for sample A and in panels (g) and (h) for sample B. An increase in the muon spin relaxation rate at low temperatures is observed for all applied pressures, indicating the presence of time-reversal symmetry breaking as seen in previous studies [8–13]. Following the previously established procedure in Ref. [13], the exponential muon spin relaxation rate λ at each temperature is obtained by fitting:

$$A_{\text{fit}}(T, t) = A_{\text{sam}} e^{-\lambda(T)t} + A_{\text{bkg}}. \quad (1)$$

A_{bkg} is a background constant to account for muons that implant into nonsuperconducting material such as cryostat walls and A_{sam} is the sample signal strength. A_{bkg} and A_{sam} are determined from weak transverse-field μ SR measurements as described in Ref. [13]. Thus, in the analysis of ZF data, λ is the sole free fitting parameter. Previously, we studied the background relaxation rate by measuring the holder without a sample [13]. We found that, within the error bars of the

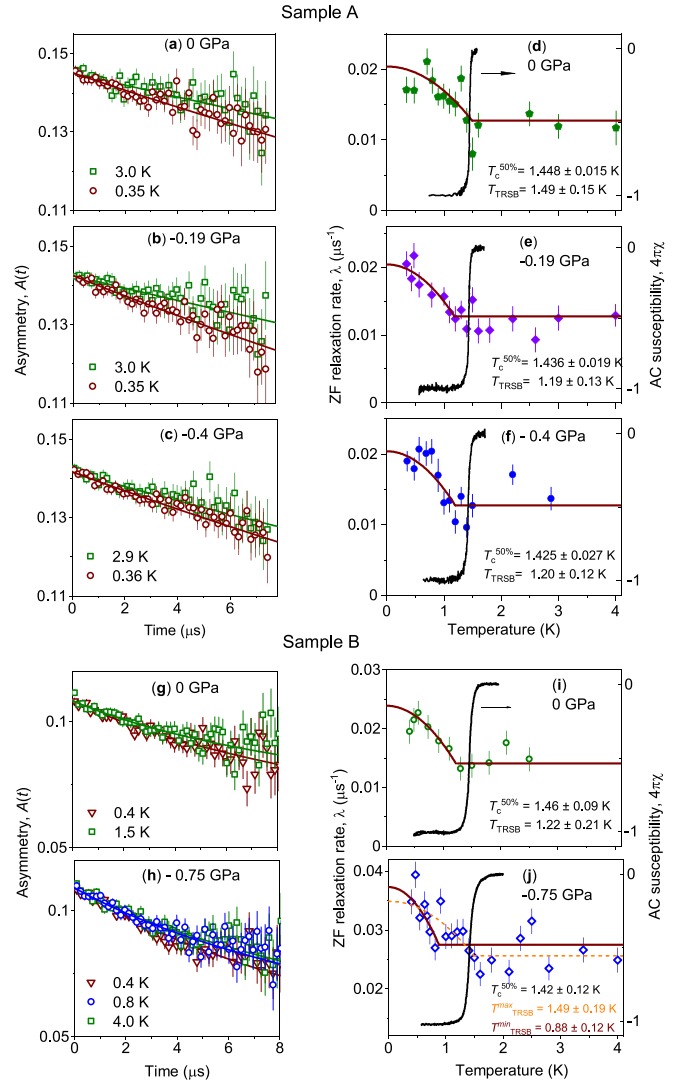


FIG. 2. (a)–(c) Sample A: Zero-field μ SR asymmetry $A(t)$ at a temperature above T_c and at the lowest temperature reached at 0 GPa, -0.19 GPa , and -0.4 GPa (110) compressive stress. (d)–(f) Temperature dependence of the muon spin relaxation rate λ (left) and magnetic susceptibility (right). The fits to $\lambda(T)$ (maroon lines) are explained in the text. Sample B: Zero-field μ SR asymmetry $A(t)$ at a temperature above and below T_c (g) zero stress and (h) -0.75 GPa (110) compressive stress. (i), (j) Temperature dependence of the muon spin relaxation rate λ (left) and *in situ* diamagnetic susceptibility data (right). Maroon solid lines are the fits to $\lambda(T)$ with b as a common fitting parameter for panels (i), (j); dashed orange curve in panel (j) is the fit with b as an individual fitting parameter. For further details, see the text.

measurements, A_{bkg} is temperature independent. However, the absolute value of the A_{bkg} is sensitive to the holder and hematite mask position.

Results for sample A at zero stress and two compressive stresses are shown in Fig. 2, panels (d)–(f). It is seen that at each stress the muon spin relaxation rate (λ) is enhanced in the superconducting state. To extract T_{TRSB} , we fit the temperature dependence of $\lambda(T)$ at each stress using a phenomenological

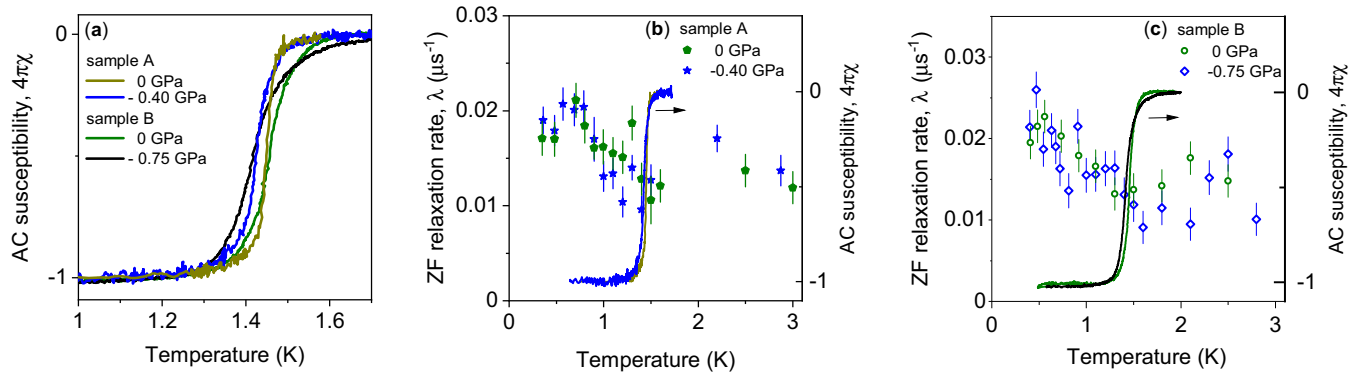


FIG. 3. (a) Comparison of the temperature dependence of the *in situ* ac susceptibility between samples A and B. (b), (c) Temperature dependencies of the muon spin relaxation rate at 0 GPa and -0.40 GPa for sample A and at 0 GPa and -0.75 GPa for sample B, plotted together. Note that the -0.75 GPa curve for sample B was shifted down for better comparison with 0 GPa data.

equation:

$$\lambda(T) = \begin{cases} \lambda_0 + b \times [1 - (T/T_{\text{TRSB}})^2], & T < T_{\text{TRSB}}, \\ \lambda_0, & T > T_{\text{TRSB}}. \end{cases} \quad (2)$$

For sample A, the b and λ_0 are taken to be common fitting parameters among all three stresses, while T_{TRSB} is obtained independently at each stress. This assumption is justified because it is the same sample at each stress and the change in T_{TRSB} is small. This fit gives $T_{\text{TRSB}} = 1.49 \pm 0.15$ K at 0 GPa, 1.19 ± 0.13 K at -0.19 GPa, and 1.20 ± 0.12 K at -0.4 GPa. To allow more direct comparison, we also show the data measured at 0 GPa and -0.4 GPa in one plot without fitted curves in Fig. 3(b).

The analysis of the data for sample B, shown in Fig. 2, panels (i) and (j), with the same model results in $T_{\text{TRSB}} = 1.22 \pm 0.21$ K at 0 GPa and 0.88 ± 0.12 K at -0.75 GPa. The rapid suppression of T_{TRSB} is consistent with the result from sample A. However, the uncertainties must be considered. For an unknown reason (possibly a shift in the sample and/or the hematite mask position), λ_0 changed substantially when stress was applied, so we had to make λ_0 a stress-dependent fitting parameter. The analysis performed in Ref. [13] indicates that λ_0 is sensitive to the precise sample configuration, which, in general, might be modified by the application of force, while b , characterizing the strength of spontaneous magnetic fields, is likely set by the defect density—it varies from sample to sample (see Ref. [12] for discussion). So the defect density is unlikely to change with stress. (At first, the measurements under stress were performed. Then the stress was slowly released at 6 K and the zero-stressed measurements were performed.) For a TRSB superconductor, the magnitude of b can also depend on the size of the superconducting gaps, and hence it might depend on T_{TRSB} and T_c values. If b is taken to be stress dependent, we obtain a larger T_{TRSB} at -0.75 GPa than at 0 GPa, as shown in panel (j) by the dashed orange curve giving a very high $T_{\text{TRSB}}^{\text{max}} = 1.49 \pm 0.12$ K. This would result in an opposite T_{TRSB} dependence on stress for sample B compared to sample A, which seems unlikely. To allow more direct comparison, we also show the data for sample B measured at 0 GPa and -0.75 GPa in one plot without fitted curves in Fig. 3(c). The -0.75 GPa curve for

sample B was shifted down for better comparison with 0 GPa data.

The resulting $T - \sigma_{110}$ experimental phase diagram is shown in Fig. 4. Since there is the discussed uncertainty in the analysis for sample B, the dashed maroon curve represents the upper limit for the $|dT_{\text{TRSB}}/d\sigma_{110}|$ slope, which substantially exceeds $|dT_c/d\sigma_{110}|$. However, with the current data, we cannot exclude the possibility that T_{TRSB} and T_c do not split under $\langle 110 \rangle$ stress.

III. DISCUSSION

Our measurements show $\frac{dT_c}{d\sigma_{110}} = 0.05 \pm 0.01$ K/GPa; T_c decreases slightly under the $\langle 110 \rangle$ compression (Fig. 4). However, uniaxial stress applied along the $\langle 110 \rangle$ direction induces not only shear strain, but also a change in unit cell volume and in the lattice parameter ratio c/a . In an analysis given in the Appendixes, these latter two effects are shown to contribute

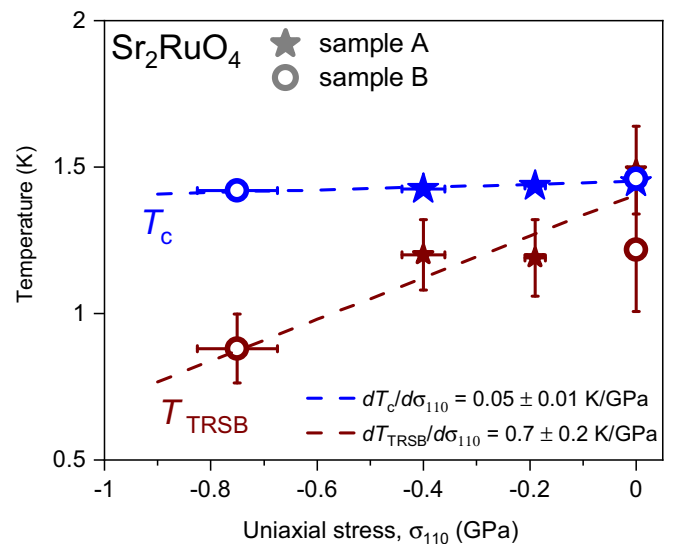


FIG. 4. Stress dependence of the superconducting and TRSB transition temperatures extracted from the experimental data together with linear fitting curves to extract $|dT_c/d\sigma_{110}|$ and the upper limit for the $|dT_{\text{TRSB}}/d\sigma_{110}|$ slope.

about 0.1 K/GPa. This sets an upper limit on the coupling of T_c to shear strain of $|\frac{dT_c}{d\epsilon_6}| \lesssim 5$ K.

Our experimental data show that T_{TRSB} can be more susceptible to the stress than T_c giving an upper limit for the slope $\frac{dT_{\text{TRSB}}}{d\sigma_{110}} \approx 0.7$ K/GPa [see Fig. 3(d)]. However, we cannot rule out the possibility that there is in fact no $\langle 110 \rangle$ stress induced splitting between T_c and T_{TRSB} . 0.7 K/GPa is much larger than the contribution from nonshear elements of the applied strain and so would require substantial coupling to the shear strain. It is shown in the Appendices that this corresponds to an upper limit $\frac{dT_{\text{TRSB}}}{d\epsilon_6} \approx \frac{1}{2} 131 \text{ GPa} (\frac{dT_c}{d\sigma_{110}} - 0.1 \text{ K/GPa}) \lesssim 40$ K.

Recently, two independent ultrasound studies of Sr₂RuO₄ reported a discontinuity in the shear elastic modulus c_{66} at T_c in accord with expectations for a multicomponent component order parameter [30,35]. If the order parameter is chiral, with two components related by symmetry ($p_x \pm ip_y$ or $d_{xz} \pm id_{yz}$), an Ehrenfest relationship applies:

$$\Delta c_{66} = -\frac{\Delta C}{T_c} \left| \frac{dT_c}{d\epsilon_6} \right| \left| \frac{dT_{\text{TRSB}}}{d\epsilon_6} \right|, \quad (3)$$

where Δc_{66} is the change in c_{66} at T_c and ΔC is the heat capacity jump at T_c [30]. We note that the ultrasound experiments are consistent with two-component order parameters that either break or do not break time-reversal symmetry. However, in light of other evidence reviewed in the Introduction, we assume that the jump in c_{66} is associated with time-reversal symmetry breaking.

In Ghosh *et al.* and Benhabib *et al.*, $\Delta c_{66} = 1.05$ and 0.03 MPa were observed, respectively [30,35]. (In Benhabib *et al.*, a change in shear sound velocity of 0.2 ppm was reported, indicating a change in c_{66} of 0.4 ppm.) The reason for the difference is not clear, although the very different frequencies of the measurements (2 versus 169 MHz) are a possible factor. Taking $\Delta C = 36$ mJ/mol K [30] in Eq. (3), $\Delta c_{66} = 1.05$ MPa implies a product of slopes $|\frac{dT_c}{d\epsilon_6}| \times |\frac{dT_{\text{TRSB}}}{d\epsilon_6}| = 2500 \text{ K}^2$ and $\Delta c_{66} = 0.03$ MPa implies a product of slopes $|\frac{dT_c}{d\epsilon_6}| \times |\frac{dT_{\text{TRSB}}}{d\epsilon_6}| = 70 \text{ K}^2$. Our data provides an upper limit on $|\frac{dT_c}{d\epsilon_6}| \times |\frac{dT_{\text{TRSB}}}{d\epsilon_6}|$ of 200 K². According to Eq. (3), the value is reconcilable with $\Delta c_{66} = 0.03$ MPa [35], but not $\Delta c_{66} = 1.05$ MPa [30].

Our data indicate that T_{TRSB} might be considerably more sensitive to $\langle 110 \rangle$ stress than T_c . If the order parameter is symmetry-protected chiral, then the ratio of heat capacity anomalies in the mean field is inverse to the ratio of slopes $|dT_c/d\epsilon_6|$ and $|dT_{\text{TRSB}}/d\epsilon_6|$ (see Supplemental Material in Ref. [13]). If the order parameter is one with accidental

degeneracy then this exact relation no longer holds, but an approximately inverse relationship between condensation energy and slopes is still expected. Our data indicate that $|dT_{\text{TRSB}}/d\epsilon_6|$ could be an order of magnitude larger than $|dT_c/d\epsilon_6|$, in which case the second heat capacity anomaly could be below the resolution limit set in Ref. [22].

Several factors affect the ratio of slopes $|dT_c/d\epsilon_6|$ and $|dT_{\text{TRSB}}/d\epsilon_6|$. For chiral states such as $d_{xz} \pm id_{yz}$ the slopes depend on the anisotropy of the Fermi surface taking part in superconductivity. In the case of multiorbital superconductivity of Sr₂RuO₄ with complex Fermi surface, the calculation of the slopes is rather challenging and requires further studies. Qualitatively, a possible explanation for a large $|dT_{\text{TRSB}}/d\epsilon_6|$ and the related small heat capacity anomaly at T_{TRSB} is that breaking time-reversal symmetry causes only a narrow node to be filled in. Recent calculations of the specific heat for various accidentally degenerate superconducting orders indicate that a better agreement between experimental data can be obtained for $s' \pm id_{xy}$, with s' indicating an s -wave state with accidental nodes, compared to other orders [36].

In conclusion, our data set an upper limit on the dependence of T_{TRSB} on shear strain ϵ_6 . This upper limit is compatible with $\Delta c_{66} = 0.03$ GPa, as reported in Ref. [35], but not with $\Delta c_{66} = 1.05$ GPa reported in Ref. [30]. Further studies under a $\langle 110 \rangle$ uniaxial stress using μ SR and other experimental techniques are needed to refine the obtained results.

ACKNOWLEDGMENTS

The work was performed at the Swiss Muon Source ($S\mu S$), Paul Scherrer Institute (PSI, Switzerland). The work of V.G. was supported by DFG GR 4667/1. The work of A.R. was supported by the Swiss National Foundation through the Ambizione Grant No. 186043. The work is supported by JSPS KAKENHI (Grants No. JP18K04715, No. JP21H01033, No. JP22H01168, and No. JP22K19093), by JSPS Core-to-Core Program (Grant No. JPJSCCA20170002), and by a JST-Mirai Program (Grant No. JPMJMI18A3). K.I. acknowledges the support from JSPS Overseas Research Fellowships. R.S. and H.-H.K. acknowledge the support from DFG SFB 1143 (Project ID No. 247310070) and the Würzburg-Dresden Cluster of Excellence on Complexity and Topology Würzburg-Dresden Cluster of Excellence on Complexity and Topology in Quantum Matter-ct.qmat (EXC 2147, Project ID No. 390858490).

APPENDIX A: ANALYSIS OF THE APPLIED STRAIN

In the experiment, we apply $\langle 110 \rangle$ stress, which results in orthorhombic distortion of the lattice and affects the unit cell parameters. In general, the applied stresses (σ_i) coupled to strains (ϵ_i) by the elasticity stiffness matrix for tetragonal crystal symmetry:

$$\begin{bmatrix} \sigma_x \\ \sigma_y \\ \sigma_z \\ \sigma_{xz} \\ \sigma_{yz} \\ \sigma_{xy} \end{bmatrix} = \begin{bmatrix} c_{11} & c_{12} & c_{13} & 0 & 0 & 0 \\ c_{21} & c_{22} & c_{23} & 0 & 0 & 0 \\ c_{31} & c_{32} & c_{33} & 0 & 0 & 0 \\ \cdot & \cdot & \cdot & c_{44} & 0 & 0 \\ \cdot & \cdot & \cdot & \cdot & c_{55} & 0 \\ \cdot & \cdot & \cdot & \cdot & \cdot & c_{66} \end{bmatrix} \begin{bmatrix} \epsilon_x \\ \epsilon_y \\ \epsilon_z \\ 2\epsilon_{xz} \\ 2\epsilon_{yz} \\ 2\epsilon_{xy} \end{bmatrix},$$

where $i = x, y, z, xz, zy,$ and xy . The shear strain in the main text is connected to the xy strain by $\epsilon_6 = 2\epsilon_{xy}$. Using the measured elastic constants from Ref. [30], we get

$$\begin{bmatrix} \sigma_x \\ \sigma_y \\ \sigma_z \\ \sigma_{xz} \\ \sigma_{yz} \\ \sigma_{xy} \end{bmatrix} = \begin{bmatrix} 243.9 & 137.7 & 85.0 & 0 & 0 & 0 \\ 137.7 & 243.9 & 85.0 & 0 & 0 & 0 \\ 85.0 & 85.0 & 257.2 & 0 & 0 & 0 \\ \cdot & \cdot & \cdot & 69.5 & 0 & 0 \\ \cdot & \cdot & \cdot & \cdot & 69.5 & 0 \\ \cdot & \cdot & \cdot & \cdot & \cdot & 65.5 \end{bmatrix} \begin{bmatrix} \epsilon_x \\ \epsilon_y \\ \epsilon_z \\ 2\epsilon_{xz} \\ 2\epsilon_{yz} \\ 2\epsilon_{xy} \end{bmatrix},$$

where the values are given in GPa. Inverting the matrix we get the relationship between strains and stresses:

$$\begin{bmatrix} \epsilon_x \\ \epsilon_y \\ \epsilon_z \\ 2\epsilon_{xz} \\ 2\epsilon_{yz} \\ 2\epsilon_{xy} \end{bmatrix} = \begin{bmatrix} 0.00624 & -0.00317 & -0.00102 & 0 & 0 & 0 \\ -0.00317 & 0.00624 & -0.00102 & 0 & 0 & 0 \\ -0.00102 & -0.00102 & 0.00456 & 0 & 0 & 0 \\ \cdot & \cdot & \cdot & 0.01439 & 0 & 0 \\ \cdot & \cdot & \cdot & \cdot & 0.01439 & 0 \\ \cdot & \cdot & \cdot & \cdot & \cdot & 0.01527 \end{bmatrix} \begin{bmatrix} \sigma_x \\ \sigma_y \\ \sigma_z \\ \sigma_{xz} \\ \sigma_{yz} \\ \sigma_{xy} \end{bmatrix}.$$

The experimental value for the slope of T_c under hydrostatic pressure is $dT_c/d\sigma_{\text{hydro}} = 0.23 \pm 0.01$ K/GPa and under uniaxial c -axis strain is $dT_c/d\sigma_z = 0.076 \pm 0.006$ K/GPa, where σ_z denotes uniaxial stress along the c axis and $\sigma_{\text{hydro}} \equiv \sigma_x = \sigma_y = \sigma_z$ hydrostatic stress, where other components are zero.

APPENDIX B: DERIVATION OF $\frac{dT_c}{d\epsilon_x}$, $\frac{dT_c}{d\epsilon_y}$, AND $\frac{dT_c}{d\epsilon_z}$

To estimate the effect of the $\langle 110 \rangle$ stress on T_c in the limit of small deformations one can decompose the effect of hydrostatic pressure and c -axis stress into individual components. To obtain the derivatives under hydrostatic pressure and c -axis stress we have used the stain-stress matrix:

$$\frac{dT_c}{d\sigma_{\text{hydro}}} = 2 \frac{dT_c}{d\epsilon_{x(y)}} \frac{d\epsilon_{x(y)}}{d\sigma_{\text{hydro}}} + \frac{dT_c}{d\epsilon_z} \frac{d\epsilon_z}{d\sigma_{\text{hydro}}} = 0.0041 \frac{dT_c}{d\epsilon_{x(y)}} + 0.00252 \frac{dT_c}{d\epsilon_z}, \quad (\text{B1})$$

$$\frac{dT_c}{d\sigma_z} = 2 \frac{dT_c}{d\epsilon_{x(y)}} \frac{d\epsilon_{x(y)}}{d\sigma_z} + \frac{dT_c}{d\epsilon_z} \frac{d\epsilon_z}{d\sigma_z} = -0.00204 \frac{dT_c}{d\epsilon_{x(y)}} + 0.00456 \frac{dT_c}{d\epsilon_z}. \quad (\text{B2})$$

Inverting the equations we get

$$\frac{dT_c}{d\epsilon_{x(y)}} = 191.3 \frac{dT_c}{d\sigma_{\text{hydro}}} - 105.72 \frac{dT_c}{d\sigma_z} \approx 35.96 \text{ K}, \quad (\text{B3})$$

$$\frac{dT_c}{d\epsilon_z} = 85.58 \frac{dT_c}{d\sigma_{\text{hydro}}} + 172.0 \frac{dT_c}{d\sigma_z} \approx 32.76 \text{ K}. \quad (\text{B4})$$

APPENDIX C: EFFECT OF THE VOLUME CHANGE AND TETRAGONAL DISTORTIONS

The effect of the hydrostatic pressure and the c -axis stress on T_c can also be decomposed on the fractional volume change of the unit cell $\epsilon_v = \Delta V/V = \epsilon_x + \epsilon_y + \epsilon_z$ and the fraction of the volume-preserving tetragonal distortion $\epsilon_{\text{tet}} = \epsilon_z - (\epsilon_x + \epsilon_y)/2$:

$$\frac{dT_c}{d\sigma_{\text{hydro}}} = \frac{dT_c}{d\epsilon_v} \frac{d\epsilon_v}{d\sigma_{\text{hydro}}} = \frac{dT_c}{d\epsilon_v} \left(\frac{d\epsilon_x}{d\sigma_{\text{hydro}}} + \frac{d\epsilon_y}{d\sigma_{\text{hydro}}} + \frac{d\epsilon_z}{d\sigma_{\text{hydro}}} \right) = 0.00662 \frac{dT_c}{d\epsilon_v}. \quad (\text{C1})$$

Thus, for the effect of the volume change, we have $\frac{dT_c}{d\epsilon_v} = 34.74$ K:

$$\frac{dT_c}{d\sigma_z} = \frac{dT_c}{d\epsilon_v} \frac{d\epsilon_v}{d\sigma_z} + \frac{dT_c}{d\epsilon_{\text{tet}}} \frac{d\epsilon_{\text{tet}}}{d\sigma_z} = \frac{dT_c}{d\epsilon_v} \left(\frac{d\epsilon_x}{d\sigma_z} + \frac{d\epsilon_y}{d\sigma_z} + \frac{d\epsilon_z}{d\sigma_z} \right) + \frac{dT_c}{d\epsilon_{\text{tet}}} \left(\frac{d\epsilon_z}{d\sigma_z} - \frac{\left(\frac{d\epsilon_x}{d\sigma_z} + \frac{d\epsilon_y}{d\sigma_z} \right)}{2} \right), \quad (\text{C2})$$

$$\frac{dT_c}{d\sigma_z} = 0.00252 \frac{dT_c}{d\epsilon_v} + 0.00558 \frac{dT_c}{d\epsilon_{\text{tet}}} = 0.08755 \text{ K/GPa} + 0.00558 \frac{dT_c}{d\epsilon_{\text{tet}}}. \quad (\text{C3})$$

Thus, for the effect of the tetragonal distortion, we have $\frac{dT_c}{d\epsilon_{\text{tet}}} = -2.07$ K. Both values are very similar to the estimated one in Ref. [37].

APPENDIX D: APPROXIMATIONS FOR THE $\langle 110 \rangle$ STRESS

For the $\langle 110 \rangle$ stress we considered two different approximations. (i) In the case of an anisotropic metal one can assume that $\sigma_{xy} = \sigma_x = \sigma_y = \sigma_{110}$ [29]. (ii) For the other limiting case, one assumes that the applied stress along the $\langle 110 \rangle$ directions results

in stress components: $\sigma_x = \sigma_y = \cos(\pi/4)\sigma_{110}$ and $\sigma_{xy} = \sigma_{110}$. To discriminate between these two possibilities we compared the experimental value of the Young's modulus along the $\langle 110 \rangle$ direction of $Y_{110} = 186.8$ GPa with the one obtained within these two approximations using the strain-stress matrix. For that, we need to express the change in the length of the diagonal d over the changes of the a axis and the angle between d and a (shear strain) $\pi/4 - \alpha$. For zero stress, $d_0 = \sqrt{2}a_0$, and under the stress, $d' = 2a' \sin(\pi/4 - \alpha)$. For the small deformations $a' \approx a_0(1 + \epsilon_x)$ and $\sin(\pi/4 - \alpha) \approx (1 - \epsilon_{xy})\sqrt{2}/2$. Thus one gets

$$\epsilon_{110} = \frac{d' - d_0}{d_0} \approx \epsilon_x - \epsilon_{xy}. \quad (D1)$$

Finally, for case (i) assuming compression we get $\sigma_{110}/Y_{110}^i = \sigma_{110}(0.01527/2 - 0.00307)$; hence $Y_{110}^i \approx 219$ GPa. For case (ii) we have $\sigma_{110}/Y_{110}^{ii} = \sigma_{110}(0.01527/2 - 0.00307/\sqrt{2})$; hence $Y_{110}^{ii} \approx 183$ GPa. The second value of $Y_{110}^{ii} \approx 183$ GPa is very close to the experimental $Y_{110} = 186.8$ GPa. Thus, for further estimations, we adopted (ii) as our approximation. In this case using Eqs. (B3) and (B4) we have

$$\frac{dT_c}{d\sigma_{110}} = 2 \frac{dT_c}{d\epsilon_{x(y)}} \frac{d\epsilon_{x(y)}}{d\sigma_{110}} + \frac{dT_c}{d\epsilon_z} \frac{d\epsilon_z}{d\sigma_{110}} + \frac{dT_c}{d2\epsilon_{xy}} \frac{d2\epsilon_{xy}}{d\sigma_{110}}, \quad (D2)$$

$$\frac{dT_c}{d\sigma_{110}} = 0.00307\sqrt{2} \frac{dT_c}{d\epsilon_{x(y)}} - \frac{0.00204}{\sqrt{2}} \frac{dT_c}{d\epsilon_z} + \frac{0.01527}{2} \frac{dT_c}{d\epsilon_{xy}} \approx 0.109 \text{ K/GPa} + 0.00764 \frac{dT_c}{d\epsilon_{xy}}. \quad (D3)$$

Alternatively, the effect of the $\langle 110 \rangle$ stress can be decomposed on the fractional volume change of the unit cell ϵ_v and the fraction of the volume-preserving tetragonal distortion ϵ_{tet} . Using Eqs. (C1) and (C2) we have

$$\frac{dT_c}{d\sigma_{110}} = \frac{dT_c}{d\epsilon_v} \frac{d\epsilon_v}{d\sigma_{110}} + \frac{dT_c}{d\epsilon_{tet}} \frac{d\epsilon_{tet}}{d\sigma_{110}} + \frac{dT_c}{d2\epsilon_{xy}} \frac{d2\epsilon_{xy}}{d\sigma_{110}} \approx 0.108 \text{ K/GPa} + 0.00764 \frac{dT_c}{d\epsilon_{xy}}, \quad (D4)$$

in a good agreement with Eq. (D3).

Hence the expected change in T_c due to shear strain is $\frac{dT_c}{d\epsilon_{xy}} = 131$ GPa ($\frac{dT_c}{d\sigma_{110}} - 0.109 \text{ K/GPa}$) ≈ -7.7 K for the measured $\frac{dT_c}{d\sigma_{110}} = 0.05(1) \text{ K/GPa}$. Finally, we assumed that the contribution to $\frac{dT_{TRSB}}{d\sigma_{110}}$ unrelated to the shear strain is 0.109 K/GPa (the same as for T_c). Therefore, we neglect this small correction in the analysis of $\frac{dT_{TRSB}}{d\sigma_{110}}$.

-
- [1] Y. Maeno, H. Hashimoto, K. Yoshida, S. Nishizaki, T. Fujita, J. G. Bednorz, and F. Lichtenberg, Superconductivity in a layered perovskite without copper, *Nature (London)* **372**, 532 (1994).
 - [2] A. Pustogow, Y. K. Luo, A. Chronister, Y.-S. Su, D. A. Sokolov, F. Jerzembeck, A. P. Mackenzie, C. W. Hicks, N. Kikugawa, S. Raghu, E. D. Bauer, and S. E. Brown, Constraints on the superconducting order parameter in Sr₂RuO₄ from oxygen-17 nuclear magnetic resonance, *Nature (London)* **574**, 72 (2019).
 - [3] K. Ishida, M. Manago, K. Kinjo, and Y. Maeno, Reduction of the 17-o knight shift in the superconducting state and the heat-up effect by nmr pulses on Sr₂RuO₄, *J. Phys. Soc. Jpn.* **89**, 034712 (2020).
 - [4] A. Chronister, A. Pustogow, N. Kikugawa, D. A. Sokolov, F. Jerzembeck, C. W. Hicks, A. P. Mackenzie, E. D. Bauer, and S. E. Brown, Evidence for even parity unconventional superconductivity in Sr₂RuO₄, *Proc. Natl. Acad. Sci. USA* **118**, e2025313118 (2021).
 - [5] M. S. Anwar, T. Nakamura, S. Yonezawa, M. Yakabe, R. Ishiguro, H. Takayanagi, and Y. Maeno, Anomalous switching in Nb/Ru/Sr₂RuO₄ topological junctions by chiral domain wall motion, *Sci. Rep.* **3**, 2480 (2013).
 - [6] T. Nakamura, T. Sumi, S. Yonezawa, T. Terashima, M. Sigrist, H. Kaneyasu, and Y. Maeno, Essential configuration of Pb/Ru/Sr₂RuO₄ junctions exhibiting anomalous superconducting interference, *J. Phys. Soc. Jpn.* **81**, 064708 (2012).
 - [7] J. Xia, Y. Maeno, P. T. Beyersdorf, M. M. Fejer, and A. Kapitulnik, High Resolution Polar Kerr Effect Measurements of Sr₂RuO₄: Evidence for Broken Time-Reversal Symmetry in the Superconducting State, *Phys. Rev. Lett.* **97**, 167002 (2006).
 - [8] G. M. Luke, Y. Fudamoto, K. M. Kojima, M. I. Larkin, J. Merrin, B. Nachumi, Y. J. Uemura, Y. Maeno, Z. Q. Mao, Y. Mori, H. Nakamura, and M. Sigrist, Time-reversal symmetry-breaking superconductivity in Sr₂RuO₄, *Nature (London)* **394**, 558 (1998).
 - [9] G. Luke, Y. Fudamoto, K. Kojima, M. Larkin, B. Nachumi, Y. Uemura, J. Sonier, Y. Maeno, Z. Mao, Y. Mori, and D. Agterberg, Unconventional superconductivity in Sr₂RuO₄, *Phys. B: Condens. Matter* **289-290**, 373 (2000).
 - [10] T. Shiroka, R. Fittipaldi, M. Cuoco, R. De Renzi, Y. Maeno, R. J. Lycett, S. Ramos, E. M. Forgan, C. Baines, A. Rost, V. Granata, and A. Vecchione, μ SR studies of superconductivity in eutectically grown mixed ruthenates, *Phys. Rev. B* **85**, 134527 (2012).
 - [11] W. Higemoto, Y. Aoki, and D. E. MacLaughlin, Spin and time-reversal symmetries of superconducting electron pairs probed by the muon spin rotation and relaxation technique, *J. Phys. Soc. Jpn.* **85**, 091007 (2016).
 - [12] V. Grinenko, D. Das, B. Zinkl, N. Kikugawa, Y. Maeno, C. W. Hicks, H.-H. Klauss, M. Sigrist, and R. Khasanov, Unsplit superconducting and time reversal symmetry breaking transitions in Sr₂RuO₄ under hydrostatic pressure and disorder, *Nat. Commun.* **12**, 3920 (2021).
 - [13] V. Grinenko, S. Ghosh, R. Sarkar, J.-C. Orain, A. Nikitin, M. Elender, D. Das, Z. Guguchia, F. Brückner, M. E. Barber, J. Park, N. Kikugawa, D. A. Sokolov, J. Bobowski, T. Miyoshi, Y. Maeno, A. P. Mackenzie, H. Luetkens, C. W. Hicks, and

- H.-H. Klauss, Split superconducting and time-reversal symmetry-breaking transitions in Sr_2RuO_4 under stress, *Nat. Phys.* **17**, 748 (2021).
- [14] B. M. Huddart, I. J. Onuorah, M. M. Isah, P. Bonfà, S. J. Blundell, S. J. Clark, R. De Renzi, and T. Lancaster, Intrinsic Nature of Spontaneous Magnetic Fields in Superconductors with Time-Reversal Symmetry Breaking, *Phys. Rev. Lett.* **127**, 237002 (2021).
- [15] C. Bergemann, A. P. Mackenzie, S. R. Julian, D. Forsythe, and E. Ohmichi, Quasi-two-dimensional fermi liquid properties of the unconventional superconductor Sr_2RuO_4 , *Adv. Phys.* **52**, 639 (2003).
- [16] H.-G. Suh, H. Menke, P. M. R. Brydon, C. Timm, A. Ramires, and D. F. Agterberg, Stabilizing even-parity chiral superconductivity in Sr_2RuO_4 , *Phys. Rev. Res.* **2**, 032023(R) (2020).
- [17] J. Clepkens, A. W. Lindquist, and H.-Y. Kee, Shadowed triplet pairings in Hund's metals with spin-orbit coupling, *Phys. Rev. Res.* **3**, 013001 (2021).
- [18] O. Gingras, R. Nourafkan, A. M. S. Tremblay, and M. Côté, Superconducting Symmetries of Sr_2RuO_4 from First-Principles Electronic Structure, *Phys. Rev. Lett.* **123**, 217005 (2019).
- [19] S. Käser, H. U. R. Strand, N. Wentzell, A. Georges, O. Parcollet, and P. Hansmann, Interorbital singlet pairing in Sr_2RuO_4 : A Hund's superconductor, *Phys. Rev. B* **105**, 155101 (2022).
- [20] S. Beck, A. Hampel, M. Zingl, C. Timm, and A. Ramires, Effects of strain in multiorbital superconductors: The case of Sr_2RuO_4 , *Phys. Rev. Res.* **4**, 023060 (2022).
- [21] A. T. Rømer, T. A. Maier, A. Kreisel, P. J. Hirschfeld, and B. M. Andersen, Leading superconducting instabilities in three-dimensional models for Sr_2RuO_4 , *Phys. Rev. Res.* **4**, 033011 (2022).
- [22] Y.-S. Li, N. Kikugawa, D. A. Sokolov, F. Jerzembeck, A. S. Gibbs, Y. Maeno, C. W. Hicks, J. Schmalian, M. Nicklas, and A. P. Mackenzie, High-sensitivity heat-capacity measurements on Sr_2RuO_4 under uniaxial pressure, *Proc. Natl. Acad. Sci. USA* **118**, e2020492118 (2021).
- [23] Y.-S. Li, M. Garst, J. Schmalian, S. Ghosh, N. Kikugawa, D. A. Sokolov, C. W. Hicks, F. Jerzembeck, M. S. Ikeda, Z. Hu, B. J. Ramshaw, A. W. Rost, M. Nicklas, and A. P. Mackenzie, Elastocaloric determination of the phase diagram of Sr_2RuO_4 , *Nature (London)* **607**, 276 (2022).
- [24] A. T. Rømer, D. D. Scherer, I. M. Eremin, P. J. Hirschfeld, and B. M. Andersen, Knight Shift and Leading Superconducting Instability from Spin Fluctuations in Sr_2RuO_4 , *Phys. Rev. Lett.* **123**, 247001 (2019).
- [25] A. T. Rømer, P. J. Hirschfeld, and B. M. Andersen, Superconducting state of Sr_2RuO_4 in the presence of longer-range Coulomb interactions, *Phys. Rev. B* **104**, 064507 (2021).
- [26] S. A. Kivelson, A. C. Yuan, B. Ramshaw, and R. Thomale, A proposal for reconciling diverse experiments on the superconducting state in Sr_2RuO_4 , *npj Quantum Mater.* **5**, 43 (2020).
- [27] G. Wagner, H. S. Røising, F. Flicker, and S. H. Simon, A microscopic Ginzburg-Landau theory and singlet ordering in Sr_2RuO_4 , *Phys. Rev. B* **104**, 134506 (2021).
- [28] R. Willa, M. Hecker, R. M. Fernandes, and J. Schmalian, Inhomogeneous time-reversal symmetry breaking in Sr_2RuO_4 , *Phys. Rev. B* **104**, 024511 (2021).
- [29] C. W. Hicks, D. O. Brodsky, E. A. Yelland, A. S. Gibbs, J. A. N. Bruin, M. E. Barber, S. D. Edkins, K. Nishimura, S. Yonezawa, Y. Maeno, and A. P. Mackenzie, Strong increase of T_c of Sr_2RuO_4 under both tensile and compressive strain, *Science* **344**, 283 (2014).
- [30] S. Ghosh, A. Shekhter, F. Jerzembeck, N. Kikugawa, D. A. Sokolov, M. Brando, A. P. Mackenzie, C. W. Hicks, and B. J. Ramshaw, Thermodynamic evidence for a two-component superconducting order parameter in Sr_2RuO_4 , *Nat. Phys.* **17**, 199 (2021).
- [31] J. S. Bobowski, N. Kikugawa, T. Miyoshi, H. Suwa, H.-S. Xu, S. Yonezawa, D. A. Sokolov, A. P. Mackenzie, and Y. Maeno, Improved single-crystal growth of Sr_2RuO_4 , *Condens. Matter.* **4**, 6 (2019).
- [32] S. Ghosh, F. Brückner, A. Nikitin, V. Grinenko, M. Elender, A. P. Mackenzie, H. Luetkens, H.-H. Klauss, and C. W. Hicks, Piezoelectric-driven uniaxial pressure cell for muon spin relaxation and neutron scattering experiments, *Rev. Sci. Instrum.* **91**, 103902 (2020).
- [33] S. Ghosh, Manipulation of time reversal symmetry breaking superconductivity in Sr_2RuO_4 by uniaxial pressure, Technische Universität Dresden, 2021.
- [34] N. Kikugawa, A. P. Mackenzie, C. Bergemann, R. A. Borzi, S. A. Grigera, and Y. Maeno, Rigid-band shift of the Fermi level in the strongly correlated metal: $\text{Sr}_{2-y}\text{La}_y\text{RuO}_4$, *Phys. Rev. B* **70**, 060508(R) (2004).
- [35] S. Benhabib, C. Lupien, I. Paul, L. Berges, M. Dion, M. Nardone, A. Zitouni, Z. Q. Mao, Y. Maeno, A. Georges, L. Taillefer, and C. Proust, Ultrasound evidence for a two-component superconducting order parameter in Sr_2RuO_4 , *Nat. Phys.* **17**, 194 (2021).
- [36] H. S. Røising, G. Wagner, M. Roig, A. T. Rømer, and B. M. Andersen, Heat capacity double transitions in time-reversal symmetry broken superconductors, *Phys. Rev. B* **106**, 174518 (2022).
- [37] F. Jerzembeck, H. S. Røising, A. Steppke, H. Rosner, D. A. Sokolov, N. Kikugawa, T. Scaffidi, S. H. Simon, A. P. Mackenzie, and C. W. Hicks, The superconductivity of Sr_2RuO_4 under c -axis uniaxial stress, *Nat. Commun.* **13**, 4596 (2022).